

Metallicities of the β Cephei stars from low-resolution ultraviolet spectra

E. Niemczura, J. Daszyńska-Daszkiewicz

Astronomical Institute, Wrocław University, ul. Kopernika 11, 51-622 Wrocław, Poland
e-mail: eniem@astro.uni.wroc.pl

Received ...; accepted ...

Abstract. We derive basic stellar parameters (angular diameters, effective temperatures, metallicities) and interstellar reddening for all β Cephei stars observed during the IUE satellite mission, including those belonging to three open clusters. The parameters are derived by means of an algorithmic procedure of fitting theoretical flux distributions to the low-resolution IUE spectra and ground-based spectrophotometric observations. Since the metallicity has a special importance for pulsating B type stars, we focus our attention in particular on this parameter.

Key words. stars: early-type - stars: abundances - stars: variables: general

1. Introduction

β Cephei variables are a well-known group of early B-type pulsating stars. Their pulsations are driven by the classical κ -mechanism, operating in the layer of metal opacity bump at $T \approx 2 \cdot 10^5$ K caused by a huge number of the absorption lines of the iron-group elements. The explanation of oscillations in these stars was possible only after the publication of the new opacity tables by Iglesias et al. (1992), and was given by Cox et al. (1992), Moskalik & Dziembowski (1992), Kiriakidis et al. (1992) and Dziembowski & Pamyatnykh (1993). As was shown by Pamyatnykh (1999), the extent of the theoretical instability domain in the H-R diagram is very sensitive to the heavy element abundance, Z . The instability domain decreases with decreasing value of Z , and for $Z \approx 0.01$ there are no unstable modes in the observed β Cephei domain. Therefore, the determination of metallicities is the first step of testing the theory of pulsational instability in massive Main Sequence stars. It would be important to fix the minimum observed value of $[m/H]$ for which the oscillations are still present in these stars. Most β Cep pulsators belong to our Galaxy, and they are supposed to have the metal abundance close to the solar value. Recently, Pigulski & Kołaczowski (2002) discovered the first extragalactic β Cep stars in LMC, where the average metallicity is much below the solar value. All LMC β Cep stars are in or close to young associations and they have probably higher metal abundance than average. Moreover,

the question "which pulsational parameters are correlated with the metal abundance?" is still open.

In this paper we analyze the IUE (*International Ultraviolet Explorer*) data combined with ground-based spectrophotometric observations of β Cephei stars. The ultraviolet (UV) part of the spectra of main-sequence B-type stars is very rich in lines of the iron-group elements. Because the greatest amount of energy for these objects is emitted in the spectral region between 1216 and 10000 Å, even the low-resolution spectra can give credible values of stellar parameters such as the effective temperature, T_{eff} , surface gravity, $\log g$, microturbulent velocity, v_t , metallicity, $[m/H]$, angular diameter, θ , and the color excess, $E(B - V)$. The usefulness of the low-resolution IUE spectra for this purpose has already been demonstrated by many authors. Fitzpatrick & Massa (1999) obtained the mean stellar parameters for fourteen main sequence stars in the spectral range O9.5 – A1. Morossi et al. (2002) used IUE spectra, combined with the visual spectrophotometric observations, to derive $[m/H]$, T_{eff} and θ for 53 objects in the solar neighborhood. In Niemczura et al. (2002) we presented the results for some objects from the paper of Code et al. (1976) and for the Magellanic Clouds B type stars, obtained by the least-squares optimization algorithm. In a previous paper (Daszyńska et al. 2002), using the above mentioned method, we determined the values of the metal abundance parameter in the atmospheres of 31 field β Cephei stars and 16 stars belonging to three open clusters NGC 3293, NGC 4755 and NGC 6231. Here we use the same data as in Daszyńska et al. (2002) but we derive the stellar parameters with the improved procedure which

allows, in particular, for a more objective error estimation. This method was applied recently by Niemczura (2003) to determine the metallicities, effective temperatures, stellar diameters and interstellar reddenings for Slowly Pulsating B-type stars.

In Sect. 2, all stars we analyze are presented and spectrophotometric observations together with their calibration are shown. The procedure of fitting the theoretical spectra to the observations and the method of bootstrap resampling adopted for determining the errors of parameters are briefly described in Sect. 3. The results and interparametric correlations are presented in Sect. 4. In Sect. 5, we discuss in detail the values of metallicities we obtained. Conclusions are given in Sect. 6.

2. The observational material

The observational material consists of IUE observations obtained with the large or small aperture. We connected the data from both the long-wavelength (LWP and LWR, 1950–3200 Å) and the short-wavelength (SWP, 1100–1950 Å) cameras. We used observations with high (0.1–0.3 Å) and low (6–7 Å) spectral resolutions. The data were processed by means of two reduction packages: IUE/NEWSIPS (*New Spectral Image Processing System*, Nichols & Linsky 1996, Gahart et al. 1997) and IUE/INES (*IUE Newly Extracted Spectra*, Rodríguez Pascual et al. 1999, González-Riestra et al. 2001 and the references therein). A detailed comparison of the IUE low-dispersion spectra extracted by the INES and NEWSIPS procedures made by Schartel & Skillen (1998) showed an excellent agreement in most cases. The main differences were found for underexposed spectra and strong spectral lines. Niemczura (2003) carried out a comparison of the IUE spectra processed by NEWSIPS and INES packages for SPB and reference stars. A similar comparison for the hotter stars made in this work gives the same results. The systematic differences appear in strong lines and at the wavelengths where the LWP/LWR and SWP spectra overlap. Large differences also occur in the wavelength range 2000 – 2300 Å for highly reddened stars. Other discrepancies are probably not systematic. As found by Niemczura (2003), better agreement exists for high-resolution data.

All data points with a flag indicating some data-quality problems were excluded from further analysis. Because of the presence of interstellar Ly α absorption, the spectral region around Ly α was omitted. The IUE observations for $\lambda > 3000$ Å were also excluded from the analysis because of the very low signal-to-noise ratio at these wavelengths. Thus, we used the IUE fluxes in the spectral range from 1300 to 3000 Å. Whenever more than one spectrum was available for a star, the observations were co-added using a cross-correlation technique. The spectra were re-binned to theoretical wavelength points.

The ultraviolet observations expressed in absolute units were supplemented by ground-based spectrophotometric measurements taken from the Breger Catalogue (Breger 1976), Pulkovo Spectrophotometric Catalogue

(Aleksieva et al. 1997), and from catalogues of Glushneva et al. (1998), Glushneva et al. (1992) and Kharitonov et al. (1988). If no spectrophotometric data were available (see Tables 1 and 2), we used Johnson *UBV* and Strömgen *wby* magnitudes. The magnitudes were converted into fluxes by means of the formula $F_\lambda = 10^{0.4(C_\lambda - m_\lambda)}$, with scaling factors C_λ taken from Gray (1998) and Bessell (1979) for the *wby* and *UBV* filters, respectively. All photometric data used in this paper were taken from the GCPD database (*General Catalogue of Photometric Data*, Mermilliod et al. 1997).

All stars selected for the analysis are presented in the Tables 1 and 2, where their names, HD numbers (ID numbers for cluster stars), numbers of IUE spectra, parallaxes and references for the ground-based observations of field objects are shown. Many β Cephei stars we analyze belong to binary or multiple systems. Some of them are wide visual binaries with separation greater than 20 arcsec and can be resolved by the IUE cameras. In this group we have eight stars: ν Eri, 12 Lac, β CMa, ξ^1 CMa, ϵ Cen, α Lup, BU Cir and γ Peg. In some cases the parameters of the companion indicate that it does not influence the spectrum of the much hotter β Cephei star.

τ^1 Lup is a visual binary with a separation of 158.2 arcsec and a difference in magnitude of 4.7, therefore the visual component does not influence the spectrum of the β Cephei star. But Proust et al. (1981) found a third component with a separation from the primary of the order of 0.3 arcsec. We have no information about this object. 27 CMa is a binary system resolved by speckle interferometry (see for example Hartkopf et al. 2000). The separation of the system is growing, the last determined value being equal to 0.133 ± 0.008 arcsec. Abt & Cardona (1984) found the orbital period of the system to be equal to $P_{orb} \approx 40$ y. θ Oph has a close companion with a separation of 0.300 ± 0.025 arcsec (Shatsky & Tokovinin 2002). BW Vul is a binary system ($P_{orb} = 33.3 \pm 0.3$ y, Pigulski 1992) with the secondary component 6 – 10 mag fainter than the primary. EN Lac is an eclipsing binary with orbital period 12.0968 d (Pigulski & Jerzykiewicz 1988, Lehmann et al. 2001 and references therein). The secondary component is fainter than the primary by about 5 mag. In all above systems there is no effect of the secondary component on the UV spectrum of the β Cephei star. The same is true for ν Cen, which is an SB system with an orbital period equal to 2.622 ± 0.018 d (Schrijvers & Telting 2002) and a separation of 5.588 ± 0.061 arcsec (Shatsky & Tokovinin 2002). Merezhin (1994) determined the masses of the components to be equal to 10.20 ± 0.10 and $1.57 \pm 0.25 M_\odot$. σ Sco is a spectroscopic binary (SB2) with a period of 33 d, and a component of a quadruple system (Pigulski 1992, Chapellier et al. 1992). The separation of the third component is equal to 0.4 arcsec and is growing (Pigulski 1992 and references therein). The brightness of this star is about 2.2 mag lower than that of the SB2 system and its orbital period is longer than 100 y (Evans et al. 1986). The fourth object in this system is separated by about 20 arcsec from the primary. β Cep is a triple

system with a distant visual component (separation equal to 13.4 arcsec). Gezari et al. (1972) found a close component, separated from the primary by about 0.25 arcsec. By 1992 this value decreased to 0.03 arcsec. The orbital elements of this system were determined by Pigulski & Boratyn (1992) who derived a period of 91.6 ± 3.7 y from the light-time effect.

In a few cases the spectra in the multiple systems are strongly influenced by the other components. β Cru has a distant visual component (separation of about 371.6 arcsec). In addition, it is a primary component of a binary system. The orbital parameters of this system were determined by Aerts et al. (1998), who derived a period of 1828.0 ± 2.5 d. The orbital parameters allowed to estimate the masses of the components, to be equal to 16 and $10 M_{\odot}$. The spectral type of the secondary is B2 V, and is consistent with the temperature of 22,000 – 23,000 K and $\log g = 4.0$ dex.

There are several spectroscopic binaries with the β Cephei variables as the primary components. α Vir has an orbital period of 4.0145 d and the primary component is the β Cephei variable. The magnitude of the secondary is lower by about 2.0 mag. The SB1 system β Cen has an orbital period of 1 y (Shobbrook & Robertson 1968), and in addition a close visual component with a separation of 1.3 arcsec and $\Delta m = 3.2$ mag. The separation in the SB1 system is 15.6 ± 2 mas (Robertson et al. 1999). Aussenloos et al. (2002), on the basis of observations of lines in the visual part of the spectrum, estimated that both components are β Cephei-type stars. κ Sco is an SB2 system with orbital period of 195 d (Molenberghs et al. 1999). The orbital parameters of the system and parameters of the components were determined by Uytterhoeven et al. (2001). Effective temperatures amount to 22,000 and 18,000 K, and the masses are equal to 17 and $12 M_{\odot}$, respectively. λ Sco is also a spectroscopic binary. The separation of the system is equal to 5.595 arcsec (De Mey et al. 1997). Heynderickx et al. (1994) estimated effective temperatures (21,200 and 23,100 K), surface gravities (3.77 and 3.76 dex) and masses (10.81 and $10.50 M_{\odot}$) of the components. From the analysis of Berghöfer et al. (2000) of IUE observations it follows that the second component is a white dwarf. This SB system also has a visual component with a separation of 1.3 arcsec and $\Delta m = 3.2$ mag.

3. The analysis

The method of analysis was presented in detail by Niemczura (2003). Here we give only brief description of the method. We analyzed low-resolution spectra by means of an algorithmic procedure of fitting the theoretical flux distributions, f_{λ}^t , to the observations, f_{λ} . The theoretical flux depends on several atmospheric parameters, like T_{eff} , $[\text{m}/\text{H}]$, $\log g$, v_t . Also the angular diameter of the star, θ and interstellar extinction described by $E(B - V)$ influenced the theoretical spectrum. We used theoretical fluxes calculated by Kurucz (1996) with the standard value of the microturbulent velocity, $v_t = 2 \text{ km s}^{-1}$. The spec-

tral resolution of the observational and theoretical data were adjusted before the analysis. To derive the vector of all parameters, we used the least-squares optimization algorithm (Bevington 1969, Press et al. 1992, Niemczura 2003).

We adopted the mean interstellar reddening curve of Fitzpatrick (1999) for the majority of the analyzed stars. For stars with high reddening ($E(B - V) > 0.10$ mag) the mean curve is not a good approximation because of spatial variability of the extinction law. In these cases we computed five additional parameters specifying the shape of the UV extinction curve (Fitzpatrick 1999). Three parameters describe the Lorentzian-like bump at 2200 Å (its width, γ , position, x_0 and strength, c_3), one is the far-UV curvature term (c_4) and the last one is the linear term (c_2).

Two additional parameters, S_1 and S_2 , were used to adjust the short- and long-wavelength parts of the IUE spectra to the visual flux level. We put $S_1 = 1$ outside the IUE/SWP region, and $S_2 = 1$ outside the wavelength region covered by the long-wavelength IUE observations. These parameters are included in the analysis for several reasons. First, for some stars we used the IUE observations made with a small aperture, and these data are not calibrated to the absolute level with high precision. Second, the flux level changes during the pulsational cycle. Third, the SWP and LWP (or LWR) observations we used were sometimes made some years apart. In such cases, errors in absolute levels caused by instrumental effects can be significant. Finally, different absolute calibrations of the UV and visual parts of the spectrum may result in a difference of levels between these two spectral ranges.

Thus, the vector of all parameters, \mathbf{p} determined simultaneously can be expressed as

$$\mathbf{p} = [T_{\text{eff}}, [\text{m}/\text{H}], \theta, E(B - V), S_1, S_2, [\gamma, x_0, c_2, c_3, c_4]].$$

We used the least-squares fitting method to determine the vector of parameters, \mathbf{p} . For more details see Niemczura (2003).

The problem of simultaneous determination of all parameters during the best-fit procedure can be solved if the parameters produce detectable and different spectral signatures. Fitzpatrick & Massa (1999) illustrated how atmospheric parameters and $E(B - V)$ affect the spectrum of a hot star and concluded that the spectral signatures produced by these parameters are different. One can therefore expect that they could be obtained simultaneously by a best-fit procedure. The same is not true for $\log g$, which cannot be obtained in many cases or is determined with a very large error.

In order to determine surface gravities in the same way for all stars, we made use of photometric calibrations and stellar evolutionary tracks. The value of $\log g$ was derived as the mean from the results from five methods, but gravities lower than 3.00 dex and greater than 4.50 dex were excluded from the mean. We used three methods that employ Strömgren photometry (Napiwotzki et al. 1993, Balona 1994, Dziembowski & Jerzykiewicz 1999) and a

method which uses the Geneva photometry (Künzli et al. 1997). In the last method, we estimated the gravities using the formula obtained from stellar evolutionary tracks. The models were computed for OPAL opacities with $X = 0.7$ and $Z = 0.02$ without taking into account the effects of rotation and convective overshooting. To this aim we considered Main Sequence evolutionary tracks for masses from 7.0 to 16.0 M_{\odot} with a step of 1 M_{\odot} . We derived the following relation:

$$\log g = -12.5894 + 4.4810 \log T_{\text{eff}} - 0.7870 \log L/L_{\odot}, \quad (1)$$

with a standard deviation equal to 0.01 dex. We found that the formulae for $Z = 0.01$ and $Z = 0.02$ give a difference in $\log g$ of the order of 0.01 dex. The luminosity, $\log L/L_{\odot}$, depends on effective temperature, stellar diameter and parallax. Here we used Hipparcos parallaxes (ESA 1997). During the best-fit procedure the current luminosity was corrected for the Lutz-Kelker bias (Lutz & Kelker 1973). The correction for the luminosity can be calculated if $\sigma_{\pi}/\pi < 0.175$. Consequently, we can determine $\log g$ by means of this method only for stars with $\sigma_{\pi}/\pi < 0.175$ (see Table 1). For the β Cephei stars in clusters, the distances d to these clusters were taken from the literature: for NGC 3293 $d = 2750 \pm 250$ pc (Baume et al. 2003), for NGC 4755 $d = 2100 \pm 200$ pc (Sanner et al. 2001) and for NGC 6231 $d = 1990 \pm 200$ pc (Baume et al. 1999). This method of determination of $\log g$ was included into the iteration process, and the values of T_{eff} and θ were calculated during the best-fit procedure. Systematic errors can be caused by such effects as the chemical composition (X, Z), convective core overshooting, rotation etc. For lower masses there may also be a problem with the treatment of stellar convection.

Formal errors of best-fit parameters resulting from the least-squares method are definitely underestimated. The technique of bootstrap resampling is probably the most useful method for estimating of confidence levels for complex least-squares solutions (Press et al. 1992, Chap. 15.6, see also Maceroni & Ruciński 1997). This technique uses the input data set, D_0 , consisting of N points, to generate simulated data sets, D_i , with the same number of points. The symbol i denotes the successive simulation. The number of all bootstrap simulations is equal to $N(\log N)^2$ (Babu & Singh 1983). In the generated data, the random fraction of original points (37% in our case) is replaced by the remaining original points by means of random resampling with replacement. The simulated data sets are analyzed in the same way as the original data. This procedure not only makes it possible to estimate reliable uncertainties of the parameters, but it can be also used for determining correlations between them.

4. Results

4.1. The field β Cephei stars

The parameters obtained for the field β Cephei stars from the IUE/NEWSIPS spectra analyzed by the bootstrap resampling method are presented in Table 3. For a few stars

(δ Cet, 19 Mon and δ Lup) the differences between the parameters obtained on the basis of the IUE data calibrated by the NEWSIPS and INES procedures exceed the error bars. In the case of δ Lup the main reason for the large discrepancy can be the low quality of the IUE data because there is only a single SWP spectrum and a single LWP/LWR spectrum. There is also only one LWP/LWR spectrum for 19 Mon. In Fig. 1 we show a comparison of the dereddened spectrum of ω^1 Sco and the theoretical spectrum resulting from the bootstrap resampling method. The theoretical spectrum was obtained for the parameters listed in Table 3. The data are plotted as a dotted line, the theoretical spectrum as a solid line. As one can see, there is a good overall agreement between these two spectra. In the inset, a closer view of the SWP part of the IUE/NEWSIPS spectrum is shown. All features of the observed spectrum are present in the theoretical fit.

Most stars we analyzed have small interstellar reddening. For stars with $E(B - V) > 0.1$ mag, the five additional parameters describing the extinction curve were determined (see Sect. 3) and are given in Table 4. For a comparison, parameters of the standard extinction curve of Fitzpatrick (1999) are also shown.

In Fig. 2 we show the β Cephei stars we analyzed in the $\log g - \log T_{\text{eff}}$ diagram. Evolutionary tracks for $M = 7, 9, 12, 16$ and $20 M_{\odot}$ are also plotted. The stellar models were computed using a standard evolutionary code written by Paczyński (1969, 1970) and improved by Sienkiewicz, Kozłowski and Pamyatnykh (private communication). We used the most recent version of OPAL opacity data (Iglesias & Rogers 1996). The effect of rotation was not taken into account. An initial hydrogen abundance $X = 0.70$ and a metal abundance $Z = 0.02$ were assumed. Two types of evolutionary tracks are shown: without the effect of convective core overshooting (solid lines), and with the overshooting effect, assuming $d_{\text{ov}} = 0.20 H_P$ (dotted lines). As one can see, all β Cephei stars are located inside the Main Sequence area.

4.2. β Cephei stars in open clusters

The parameters obtained for β Cephei stars belonging to the galactic open clusters NGC 3293, NGC 4755 and NGC 6231 are shown in Table 3. The analysis was performed for six members of NGC 3293, five members of NGC 4755, and five of NGC 6231. For a few stars (NGC 3293-14, NGC 4755-7, NGC 4755-10, NGC 4755-228, NGC 4755-332, NGC 6231-238, NGC 6231-937) the values of parameters obtained from the two sets of data, IUE/NEWSIPS and IUE/INES, do not agree to within their errors. This is mainly caused by the poor quality of the IUE data.

The reddening is in all cases greater than 0.10 mag, so that there is a need to use a specified extinction curve. The extinction curves for stars belonging to NGC 3293 and NGC 6231 were taken from Massa & Fitzpatrick

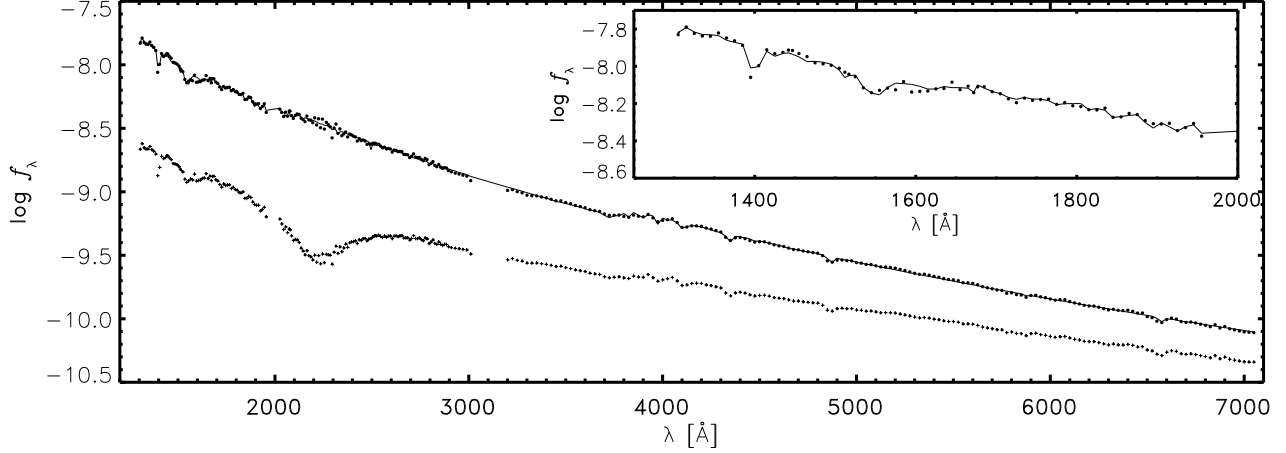


Fig. 1. Dereddened stellar energy distribution of ω^1 Sco (*dotted line*) in comparison with the best-fit model (*solid line*). The original flux of ω^1 Sco is also shown (*crosses*). The IUE data were calibrated by means of the NEWSIPS reduction package. In the inset, there is a closer view of the short-wavelength part of the spectrum.

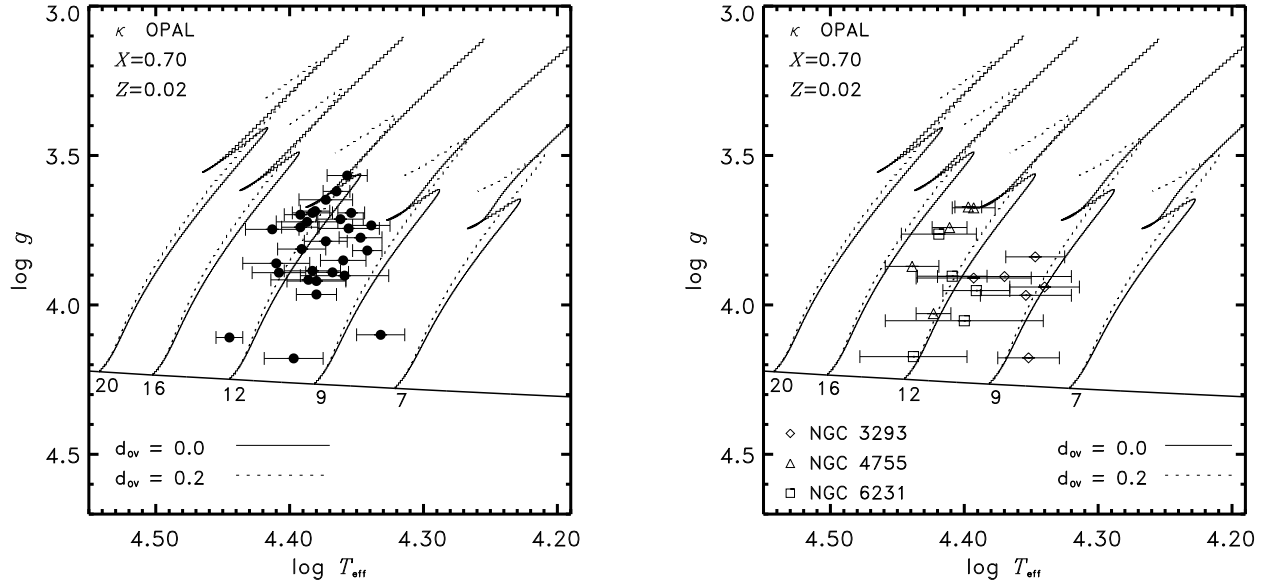


Fig. 2. The position of the field β Cep stars (left panel) and those from the three open clusters (right panel) on the $\log g$ vs. $\log T_{\text{eff}}$ diagram. The evolutionary tracks were calculated without (solid line) and with (dotted line) taking into account the effect of convective core overshooting. We assumed $d_{\text{ov}} = 0.2$.

(1988), while for NGC 4755 the standard extinction curve of Fitzpatrick (1999) was used.

The study of β Cephei stars in open clusters is important because their location in the colour-magnitude diagram indicates their evolutionary state. There are eleven open clusters in which β Cephei variables were discovered (a recent example: three β Cep stars in NGC 6910, Kołaczkowski et al. 2004). A still unexplained problem is why some young clusters contain those variables and others, like NGC 2362 (Balona & Laney 1995), do not. The other problem is the difference in location of the instability strips for various clusters of nearly the same age. According to Balona & Koen (1994), the location of the β Cephei variables belonging to NGC 4755 on the HR diagram is shifted to lower effective temperatures compared

to NGC 3293. However, we obtained opposite results: the location of β Cephei stars in NGC 4755 is shifted to the higher effective temperatures as compared to NGC 3293. In the case of NGC 4755 we found lower values of $[m/H]$ than in the case of NGC 3293. For the lower metallicity the ZAMS line is shifted to the left in the H-R diagram, thus our results are fully consistent.

4.3. Correlations between the parameters

The mean correlations, ρ_{mean} , their standard deviations, σ_{ρ} , median values, ρ_m , and ranges of correlation coefficients for the β Cephei stars are presented in Table 5. Because of the subject of this work, the most interesting are the correlations between metallicity and other param-

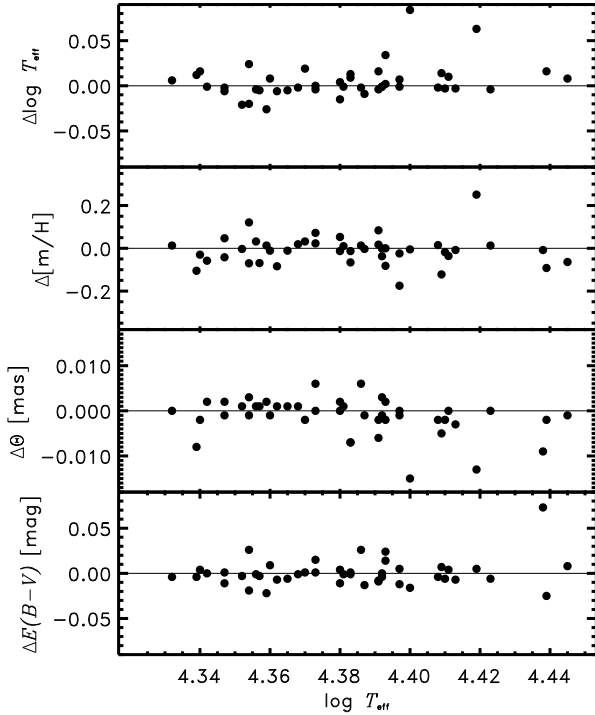


Fig. 3. Differences in parameters, $\Delta p_i = p_i(\text{NEWSIPS}) - p_i(\text{INES})$, as a function of the effective temperature obtained from the INE/NEWSIPS data.

eters obtained simultaneously. The values of ρ_{mean} and ρ_m for metallicity are small and amount to about 0.2. Also the standard deviations are small, which means that even for individual objects correlations are not large. Small values of ρ_{mean} indicate that the metal abundance, $[\text{m}/\text{H}]$, is not correlated with the other parameters and can be determined from the best-fit procedure with good precision. The correlations between the other parameters are larger. The effective temperature is strongly correlated with the interstellar reddening, $\rho_{\text{mean}} = 0.73$. A lower value of ρ_{mean} was obtained for effective temperature and stellar diameter. The smallest correlation was found between $\log T_{\text{eff}}$ and $[\text{m}/\text{H}]$. The correlations can be strong for individual objects. Somewhat lower values of ρ_{mean} and ρ_m are found between θ and other parameters; the largest value of the mean correlation is obtained for θ and $\log T_{\text{eff}}$ (0.66), and the lowest one, as in the other cases, between θ and $[\text{m}/\text{H}]$ (0.23). The correlations between interstellar reddening and others parameters are lower in the last case. The largest correlation was obtained between $E(B-V)$ and $\log T_{\text{eff}}$, while the lowest between $E(B-V)$ and $[\text{m}/\text{H}]$.

4.4. Comparison between NEWSIPS and INES

In Fig. 3 we plot the differences between the parameters obtained from the IUE data calibrated with the NEWSIPS and INES procedures, $\Delta p_i = p_i(\text{NEWSIPS}) - p_i(\text{INES})$, as a function of $\log T_{\text{eff}}$. In the four panels we can see these differences for $\log T_{\text{eff}}$, θ , $[\text{m}/\text{H}]$ and $E(B-V)$. For the

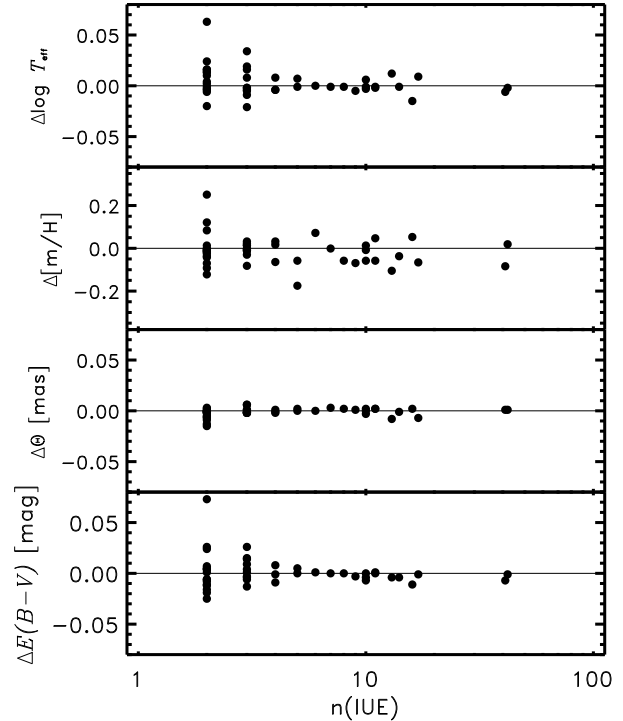


Fig. 4. The same as in Fig. 3, but as a function of the number of IUE spectra, $n(\text{IUE})$.

small range of effective temperature shown in the Fig. 3 there is no correlation between Δp_i and $\log T_{\text{eff}}$.

Small mean differences, $\langle |\Delta \mathbf{p}| \rangle$, were found for all parameters, that is 0.014 ± 0.001 for $\log T_{\text{eff}}$ ($\sigma = 0.023$), 0.003 ± 0.0001 ($\sigma = 0.003$) for θ , 0.046 ± 0.001 ($\sigma = 0.050$) for $[\text{m}/\text{H}]$ and 0.010 ± 0.001 ($\sigma = 0.012$) for $E(B-V)$. For all this mean values, the standard deviations are quite large. This means that the differences for individual objects can be significant.

In Fig. 4 we show the same differences, Δp_i , as a function of the number of available IUE spectra. As one could expect, the largest differences are obtained for stars with at most two spectra available from each IUE camera. When the number of the IUE spectra grows, the scatter of $\Delta \mathbf{p}$ decreases.

5. Discussion of the parameter $[\text{m}/\text{H}]$

5.1. General properties

The metallicities of the β Cephei stars determined from the IUE/NEWSIPS spectra range from -0.47 ± 0.18 dex for 27 CMa to $+0.21 \pm 0.09$ dex for HN Aqr. The extreme values determined from the IUE/INES data were obtained for τ^1 Lup and, again, HN Aqr; they are equal to -0.42 ± 0.17 dex and $+0.20 \pm 0.10$ dex, respectively. The distribution of the $[\text{m}/\text{H}]$ parameter resulting from NEWSIPS and INES spectra is shown in Fig. 5. These two samples follow normal distributions within the error limits. Applying the one-way Anova statistical test we ob-

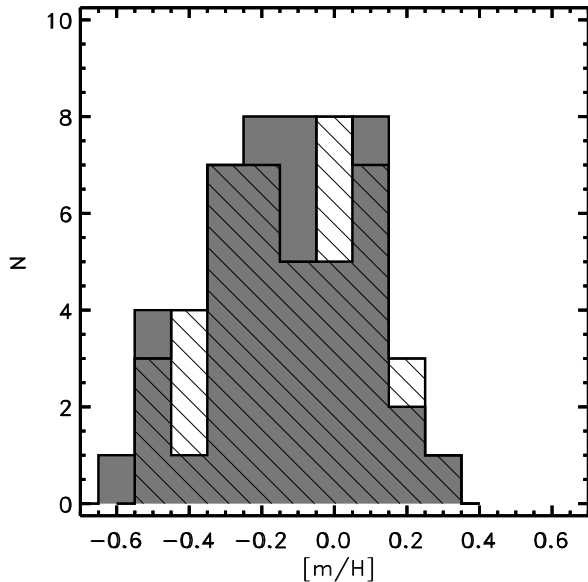


Fig. 5. The distribution of the β Cephei stars with the $[m/H]$ parameter. The hatched histogram shows the results obtained from the IUE/NEWSIPS data, while the gray one presents results obtained from the IUE/INES data.

tained that the two means are not significantly different up to the significance level of $\alpha = 0.83$. Thus we conclude that there is no difference between the values of $[m/H]$ found from the IUE data processed by both reduction packages. The mean value of the metal abundance parameter for the β Cephei stars is equal to -0.13 ± 0.03 dex and -0.14 ± 0.03 dex for IUE/NEWSIPS and IUE/INES, respectively. The mean metallicity for the field β Cephei stars is equal to -0.14 ± 0.03 dex (IUE/NEWSIPS) and -0.13 ± 0.03 dex (IUE/INES). The mean values of the metal abundance parameter for the cluster stars, obtained from the analysis of IUE/NEWSIPS spectra is equal to $+0.05 \pm 0.06$ dex for NGC 3293, -0.43 ± 0.05 dex for NGC 4755 and -0.01 ± 0.06 dex for NGC 6231. From the IUE/INES spectra we obtained nearly the same values: $+0.08 \pm 0.04$ dex for NGC 3293, -0.40 ± 0.06 dex for NGC 4755 and -0.05 ± 0.05 dex for NGC 6231. These determinations are consistent with our previous results (Daszyńska et al. 2002), obtained with a less accurate method.

Metal abundances of hot stars in the solar vicinity lower by about 0.20 dex than the solar value were reported by Gies & Lambert (1992, hereafter GL92), Cunha & Lambert (1994), Kilian (1992), Kilian et al. (1994), Daflon et al. (1999), Gummersbach et al. (1998), Niemczura (2003), and others. These results were obtained from both high- and low-resolution data. All quoted authors used Kurucz's ATLAS models of stellar atmospheres. Metal abundances obtained in the present paper from the low-resolution IUE observations are in agreement with these results.

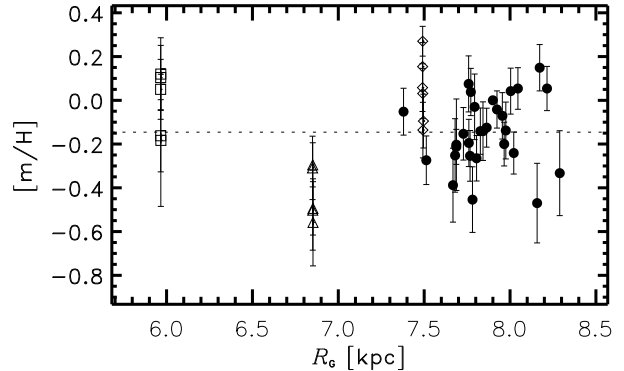


Fig. 6. The distribution of the metallicity parameter of the β Cephei stars from the IUE/NEWSIPS data as a function of the galactocentric distance (in kpc). The dashed line indicates the mean value of $[m/H]$ obtained for all β Cephei stars. Symbols are the same as in Fig. 2.

In Fig. 6 we present the dependence of $[m/H]$ on the galactocentric distance. The distance for the field stars were calculated by using the Hipparcos parallaxes (ESA 1997). For the stars from open clusters we assumed the same values of the distance from the Sun as in Chapter 3. The galactocentric distance of the Sun, $R_{G,\odot} = 7.9$ kpc was adopted from McNamara et al. (2000). As can be seen from the figure, the field stars are spread over a small range of about 0.5 kpc in galactocentric distance, so that no clear indication of a metallicity gradient is apparent. However, we would like to point out that some intrinsic scatter of the metallicity is certainly present.

5.2. Comparison with the literature

For eleven β Cephei stars in our sample, the metallicity has been determined by other authors.

One of the well-studied β Cephei stars is γ Peg. The majority of determinations was obtained from the visual part of the spectrum. Snijders (1969) determined $[Fe/H]$ to be equal to $+0.48$ dex, while Peters (1976) found a much lower iron abundance, equal to $+0.04$ dex. GL92 obtained $[FeII/H] = +0.29$ dex and Pintado & Adelman (1993) found $[Fe/H] = +0.04$ dex. From the high-resolution ultraviolet IUE spectra, Proffitt & Quigley (2001, hereafter PQ2001) determined $[Fe/H] = -0.15$ dex. The values of $[m/H]$ obtained by us, -0.04 ± 0.09 dex and $+0.02 \pm 0.10$ dex, are then consistent with the determinations of Peters (1976) and Pintado & Adelman (1993).

The differences between the values of metal abundances for For 16 Lac determined by different authors are significant. GL92 obtained the iron abundance equal to -0.23 dex from the visual part of the spectrum, while from the UV spectrum PQ2001 obtained $[Fe/H] = -0.09$ dex, and Venn et al. (2002) found $[m/H] = +0.16 \pm 0.18$ dex. Recently, Thoul et al. (2003) determined the abundances of the elements from the visual part of the spectrum. According to these authors, the iron abundance amounts to -0.08 ± 0.09 dex. Our values are consistent with the

last results to within the errors of determination: $[m/H] = -0.14 \pm 0.13$ dex and -0.15 ± 0.14 dex.

For δ Cet GL92 determined the iron abundance to be equal to -0.24 dex from the analysis of the visual part of the spectrum. Different values were obtained from the ultraviolet spectra. From the IUE spectra PQ2001 determined $[Fe/H]$ to be equal to -0.15 dex. Venn et al. (2002), from HST/STIS spectrograph data, found $[m/H] = -0.15 \pm 0.15$ dex. All these determinations are in agreement with the present work. For 15 CMa and β Cep the metal abundances were determined by the same authors. GL92 found $[Fe/H] = -0.47$ dex from the visual part, while from the analysis of the UV data, PQ2001 and Venn et al. (2002) obtained -0.13 dex and $+0.10 \pm 0.10$ dex, respectively. The values we found are close to the latter determinations. The metal abundances derived for β Cep range from -0.31 dex (PQ2001) to -0.16 ± 0.23 dex (Venn et al. 2002). Both these values were determined from the UV spectra. From the lines in the visual part of the spectrum, GL92 obtained $[Fe/H] = -0.23$ dex. The values of $[m/H]$ obtained by us are equal to -0.07 ± 0.11 dex and -0.01 ± 0.09 dex, respectively.

For the rest of the β Cephei stars there are only two or one determination of the metal abundances in the literature. Recently, Stankov et al. (2003) announced a determination of the abundances of elements for BW Vul, derived from high-resolution spectra in the blue. According to these authors, the iron abundance, $[Fe/H]$, amounts to $+0.02$ dex. This is close to the value obtained by us, $[m/H] = +0.09 \pm 0.02$ dex.

For PHL 346, the first abundance determination was done by Ryans et al. (1996). From visual part of the spectrum, the authors obtained $[Fe/H] = -0.84$ dex. Ramspeck et al. (2001), from the same spectral range, determined a much higher value of the iron abundance, $[Fe/H] = -0.12$ dex. In this work, $[m/H] = +0.21 \pm 0.09$ dex (IUE/NEWSIPS) and $+0.20 \pm 0.10$ dex (IUE/INES) were obtained. The metallicities obtained in the present paper for β Cru are consistent with the values given by Kilian (1994), $[Fe/H] = -0.08$ dex (from the visual part of the spectrum) and PQ2001, $[Fe/H] = -0.25$ dex. For BU Cir, the values determined in this work are lower than the iron abundance, $[Fe/H] = -0.12$ dex, given by Kilian (1994). For the following four stars, the values obtained from the visual part of the spectrum are taken from GL92, while the UV data were analyzed by PQ2001. Our metallicities of ν Eri are close to the $[Fe/H] = -0.08$ dex given by GL92, but the iron abundance determined by PQ2001 is lower, namely -0.27 dex.

For ξ^1 CMa we obtained metallicities close to the iron abundance of -0.30 dex determined by PQ2001. The values obtained in this paper are also consistent within the error limits with $[Fe/H] = -0.18$ dex obtained by GL92. For β CMa we obtained $[m/H] = +0.04 \pm 0.11$ dex and $+0.08 \pm 0.11$ dex from the IUE/NEWSIPS and IUE/INES data, respectively. However, GL92 determined $[Fe/H] = -0.41$ dex and PQ2001 found that $[Fe/H] = -0.22$ dex. In the case of 12 Lac, the values determined in this paper:

-0.20 ± 0.10 dex (IUE/NEWSIPS) and -0.22 ± 0.10 dex (IUE/INES) are higher than the iron abundance obtained by GL92, -0.41 dex. The iron abundance found by PQ2001 is equal to -0.08 dex.

5.3. Metallicity and pulsations

In Fig. 7 we show the instability domain of β Cephei variables for three values of the metal abundance, $Z = 0.01, 0.015, 0.02$, and the stars we analyzed. As before, the field β Cep stars and those belonging to the three open clusters are plotted in separated panels. The majority of field β Cephei stars is located within the instability region defined by $Z = 0.015$. Only for three stars are the values of surface gravity higher than 4.0 dex. Two stars, 27 CMa and ω^1 Sco, are located outside the instability regions. The metallicity parameters, $[m/H]$, for both are lower than -0.40 dex. This is not a surprise as 27 CMa is a Be star. In the case of ω^1 Sco there is also the possibility that it is a ζ Oph-type variable.

To check which pulsational parameter is sensitive to the metallicity in β Cep stars, in Fig. 8 we plot the period of the dominant mode, P , radial velocity amplitude, $2K$, its light amplitude in the V filter, A_V , and a ratio of photometric amplitudes, A_{U-B}/A_V , as a function of the $[m/H]$ parameter. We note that the last quantity is independent of the inclination angle, i , and the intrinsic pulsational amplitude, ε . We have checked all passbands and colors available in the literature, and here we give representative examples. Panel *a* of Fig. 8 is for the pulsational periods, the values of which are marked as filled circles for the field β Cep stars, and as diamonds, triangles and squares for β Cephei stars in the clusters NGC 3292, NGC 4755 and NGC 6231, respectively. As one can see, there is no correlation between metallicity and mentioned pulsational parameters, as was already pointed out by Daszyńska et al. (2002).

Also the projected rotational velocity, $v_e \sin i$, is not correlated with the metallicity parameter.

In our previous papers (Daszyńska 2001, Daszyńska et al. 2003) we stated that the mean metallicity parameter, $[m/H]$, is higher in the case of multiperiodic β Cep stars than in the case of monopерiodic variables. Here we confirm this result. The mean value of the $[m/H]$ parameter for multiperiodic β Cep stars amounts to -0.07 ± 0.03 dex, while the mean metallicity for monopерiodic variables is equal to -0.26 ± 0.06 dex. This result is in agreement with the nonadiabatic pulsational theory which predicts a larger number of unstable modes for higher values of the metal abundance.

The dichotomy of β Cep stars with regard to metallicity is discussed in detail in a separate paper (Daszyńska-Daszkiewicz & Niemczura 2004).

6. Conclusions and prospects

We derived basic stellar parameters such as the effective temperature, gravity, angular diameter, metallicity and

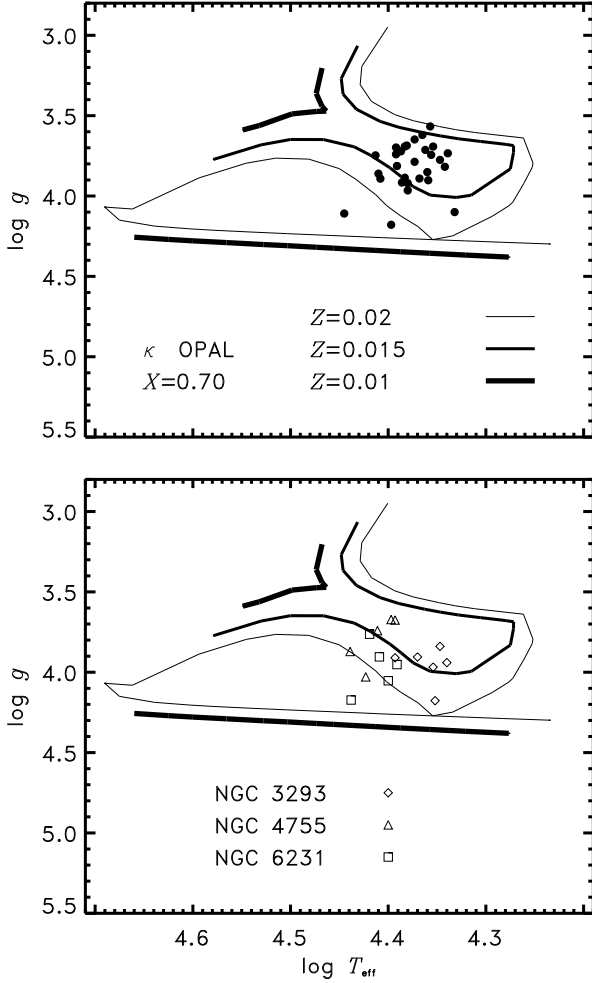


Fig. 7. The location of the β Cephei stars on the $\log g$ vs. $\log T_{\text{eff}}$ diagrams. The instability regions for $Z = 0.02$, 0.015 and 0.01 were taken from Pamyatnykh (1999). In the upper panel the position of the field β Cephei stars is shown, while in the lower one, the position of variables from the open clusters.

interstellar reddening for all β Cep stars monitored by the International Ultraviolet Explorer satellite. Among them there were field β Cep stars and variables belonging to three young open clusters: NGC 3293, NGC 4755 and NGC 6231. The mean values of the $[m/H]$ parameter for the β Cephei stars are equal to -0.13 ± 0.03 dex and -0.14 ± 0.03 dex for IUE/NEWSIPS and IUE/INES data, respectively. The mean metallicity for the field β Cephei variables is equal to -0.14 ± 0.03 dex (IUE/NEWSIPS) and -0.13 ± 0.03 dex (IUE/INES), while the mean values of $[m/H]$ for the cluster stars obtained from the analysis of IUE/NEWSIPS spectra are equal to $+0.05 \pm 0.06$ dex for NGC 3293, -0.43 ± 0.05 dex for NGC 4755 and -0.01 ± 0.06 dex for NGC 6231. From the IUE/INES spectra, we obtained nearly the same values: $+0.08 \pm 0.04$ dex for NGC 3293, -0.40 ± 0.06 dex for NGC 4755 and

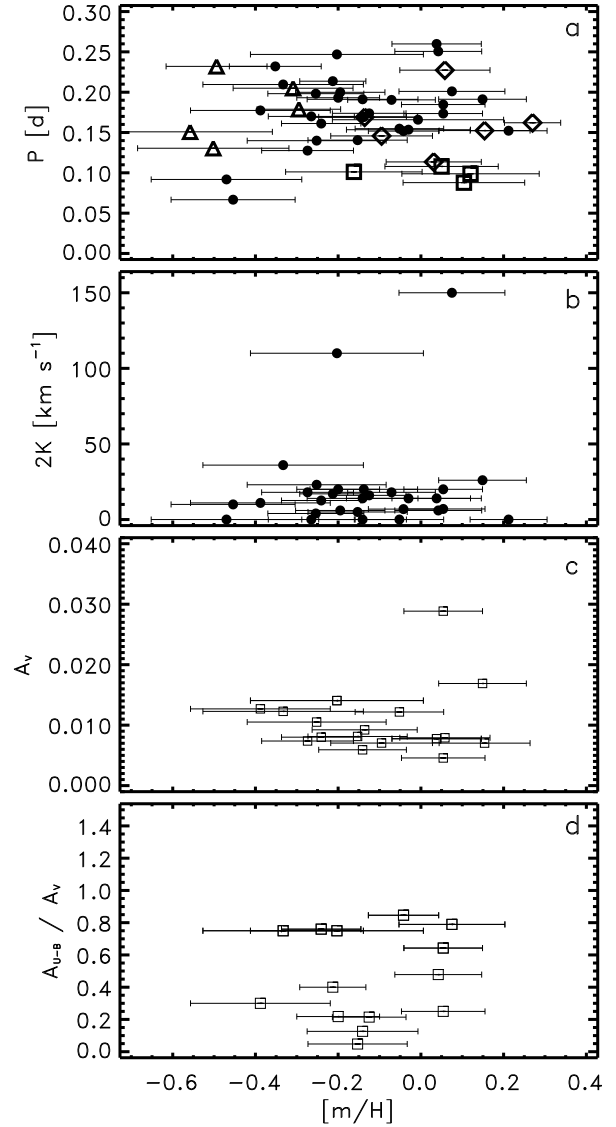


Fig. 8. Dependence of pulsational parameters: P , $2K$, A_V and A_{U-B}/A_V on the metallicity parameter, $[m/H]$.

-0.05 ± 0.05 dex for NGC 6231. These values are consistent with our previous results (Daszyńska et al. 2002), obtained with the less accurate method.

The values of the metallicity parameter we obtained, are not correlated with any pulsational parameter or the projected rotational velocity. However, we have noticed that, on the whole, multiperiodic variables have higher values of metallicity than the monopерiodic ones. This is consistent with pulsation theory.

The abundance of metals, especially that of iron, in β Cephei variables is one of the fundamental parameters. In the case of main-sequence B stars, metallicities, $[m/H]$, obtained from the UV spectra give mainly an estimation of $[Fe/H]$.

The value of $[\text{Fe}/\text{H}]$ in the Kurucz's models is larger than in the widely used in the pulsation theory OPAL and OP data. One can therefore expect that $[\text{Fe}/\text{H}]$ determined using the ATLAS9 models should be lower in comparison with $[\text{Fe}/\text{H}]$ obtained on the basis of the OPAL or OP data (see also Fitzpatrick & Massa 1999). To compare observational metallicities of the stars with the values resulting from the theory, we have to include the correction for $[\text{m}/\text{H}]$ of about 0.12 dex. The metallicities of the β Cep stars predicted by the theory of pulsations are not in contradiction with most values determined by us. Pamyatnykh (1999) showed that the β Cephei instability strip vanishes for $Z \approx 0.01$, corresponding to $[\text{m}/\text{H}] \approx -0.30$ dex, and to $[\text{m}/\text{H}] \approx -0.42$ dex from the Kurucz's fluxes. There are several stars with metallicity parameter lower than this limit. But we have to remember that our values give information about photospheric metal abundances. Some other effects which we did not take into account such as diffusion or element mixing may also be important. Besides, we used a standard mixture of elements. Nevertheless, our results provide important information about the metallicity range for these pulsating stars. In particular, because there is a problem with the estimation of the $[\text{m}/\text{H}]$ parameter for early type stars from photometry, making use of low-resolution ultraviolet spectra seems up to now the best and fastest way to determine the metallicity of B-type pulsating variables.

However, for asteroseismological purposes, there is a need for a detailed analysis of chemical composition, because oscillation frequencies are very sensitive to the adopted mixture, and this is the aim of our future work.

Acknowledgements We thank prof. Dziembowski and prof A. Pamyatnykh for permission of using the evolution code and non-adiabatic pulsation code.

References

- Abt, H.A., & Cardona, O., 1984, ApJ, 285, 190
Aerts, C., De Cat, P., Cuypers, J., et al. 1998, A&A, 329, 139
Alekseeva, G.A., Arkharov, A.A., Galkin, V.D. et al. 1997, Baltic Astron., 6, 481
Ausseloos, M., Aerts, C., Uytterhoeven, K., et al., 2002, A&A, 384, 209
Babu, G.J., & Singh, K. 1983, Annals. Statist., 11, 999
Balona, L.A. 1994, MNRAS, 268, 119
Balona, L.A., & Koen, C., 1994, MNRAS, 267, 1071
Balona, L.A., & Laney, C.D., 1995, MNRAS, 276, 627
Baume, G., Vázquez, R.A., & Feinstein, A., 1999, A&AS, 137, 233
Baume, G., Vázquez, R.A., Carraro, G., & Feinstein, A., 2003, A&A, 402, 549
Berghöfer, T.W., Vennes, S. & Dupuis, J., 2000, ApJ, 538, 854
Bessel, M.S. 1979, PASP, 91, 589
Bevington, P.R. 1969, in Data Reduction and Error Analysis for the Physical Science, New York: McGraw-Hill
Bogges, A., Carr, F.A., Evans, D.C., et al. 1978, Nature, 275, 372
Breger, M. 1976, ApJ, 32, 7
Chapellier, E., Sadsaound, H., Valtier, J.C., et al. 1998, A&A, 331, 1046
Code, A.D., Bless, R.C., Davis, J., & Brown, R.H. 1976, ApJ, 203, 417
Cox, A.N., Morgan, S.M., Rogers, F.J., & Iglesias, C.A., 1992, ApJ, 393, 272
Cunha, K., & Lambert, D.L. 1994, ApJ, 426, 170
Daflon, S., Cunha, K., & Becker, S.R. 1999, ApJ, 522, 950
Daszyńska, J., Niemczura, E., & Cugier, H. 2002, Adv. Space Res. 31, 387
Daszyńska-Daszkiewicz, J., Niemczura, E., 2004, this issue
De Mey, K., Aerts, C., Waelkens, C., Cranmer, S.R., et al., 1997, A&A, 324, 1096
Dziembowski, W.A., & Jerzykiewicz, M., 1999, A&A, 341, 480
Dziembowski, W.A., & Pamyatnykh, A.A. 1993, MNRAS, 262, 204
ESA 1997, The Hipparcos and Tycho Catalogues
Evans, D.S., McWilliam, A., Sandmann, W.H., & Frueh, M., 1986, AJ, 92, 1210
Fitzpatrick, E.L. 1999, PASP, 111, 63
Fitzpatrick, E.L., & Massa, D. 1999, ApJ, 525, 1011
Gahart, M.P., Smith, M.A., Levay, K.L., & Thompson, R.W. 1997, IUE NEWSIPS Information Manual, Version 2.0
Gezari, D.Y., Labeyrie, A., & Stachnik, R.V., 1972, ApJ, 171L, 67
Gies, D.R., & Lambert, D.L. 1992, ApJ, 387, 673
Glushneva, I.N., Kharitonov, A.V., Knyazeva, L.N., & Shenavrin, V.I., 1992, A&AS, 92, 1
Glushneva, I.N., Doroshenko, V.T., Fetisova, T.S., 1998, *Spectrophotometric Catalog of Stars of the Sternberg State Astronomical Institute.*, CDS Catalogues, III/208
González-Riestra, R., Cassatella, A., & Wemsteker, W. 2001, A&A, 373, 730
Gray, R.O. 1998, ApJ, 116, 482
Gummersbach, C.A., Kaufer, D.R., Schäfer, D.R., et al. 1998, A&A, 338, 883
Hartkopf, W.I., Mason, B.D., McAlister, H.A., et al., 2000, AJ, 119, 3084
Heynderickx, D., Waelkens, C., & Smeyers, P., 1994, A&AS, 105, 447
Iglesias, C.A., Rogers, F.J., & Wilson, B.G. 1992, ApJ, 397, 717
Iglesias, C.A., & Rogers, F.J. 1996, ApJ, 464, 943
Kharitonov, A.V., Tereshchenko, V.M., & Knyazeva, L.N., 1988, Alma-Ata, Nauka, p. 484
Kilian, J. 1992, A&A, 262, 171
Kilian, J. 1994, A&A, 282, 869
Kilian, J., Montenbruck, O., & Nissen, P.E. 1994, A&A, 28 4, 437
Kiriakidis, M., El Eid, M.F., & Glatzel, W., 1992, MNRAS, 255, 1P
Kołaczkowski, Z., Pigulski, A., Kopacki, G., & Michalska, G., 2004, 2004, *Acta Astron.*, 54, 33
Kurucz, R. 1996, CD-ROM, No. 13 and 19
Künzli, M., North, P., Kurucz, R.L., & Nicolet, B. 1997, A&AS, 122, 51
Lehmann, H., Harmanec, P., Aerts, C., et al., 2001, A&A, 367, 236
Lutz, T.E., & Kelker, D.H. 1973, PASP, 85, 573
Maceroni, C., & Ruciński, S.M. 1997, PASP, 109, 782
Massa, D., Fitzpatrick, E.L., 1986, ApJS, 60, 305
McNamara, D.H., Madsen, J.B., Barnes, J., & Ericksen, B.F. 2000, PASP, 112, 202

- Merezhin, U.P., 1994, *Ap&SS*, 215, 83
- Mermilliod, J.C., Mermilliod, M., & Hauck, B. 1997, *A&AS*, 124, 349
- Molenberghs, G., Aerts, C., & De Cat, P., 1999, *A&AS*, 135, 383
- Morossi, C., Di Marcantonio, P., Franchini, M., et al. 2002, *ApJ*, 577, 377
- Moskalik, P., & Dziembowski, W.A., 1992, *A&A*, 256, L5
- Napiwotzki, R., Schönberner, D., & Wenske, V. 1993, *A&A*, 268, 653
- Nichols, J.S., & Linsky, J.L. 1996, *AJ*, 111, 517
- Niemczura, E., Daszyńska, J., & Cugier, H. 2002, *Adv. Space Res.* 31, 399
- Niemczura, E. 2003, *A&A*, 404, 689
- Paczyński, B., 1969, *Acta Astron.*, 19, 1
- Paczyński, B., 1970, *Acta Astron.*, 20, 47
- Pamyatnykh, A.A. 1999, *Acta Astron.*, 49, 119
- Peters, G.J., 1976, *ApJS*, 30, 551
- Pigulski, A., & Kołaczkowski, Z., 2002, *A&A*, 388, 88
- Pigulski, A., 1992, *A&A*, 261, 203
- Pigulski, A., 1992, PhD Thesis, Wrocław University
- Pigulski, A., & Boratyn, D.A., 1992, *A&A*, 253, 178
- Pigulski, A., & Jerzykiewicz, M., 1988, *Acta Astron.*, 38, 401
- Pintado, O.I., & Adelman, S.J. 1993, *MNRAS*, 264, 63
- Press, W.H., Teukolsky, S.A., & Vetterling, W.T. 1992, *Numerical Recipes in Fortran*, 2nd ed. (Cambridge and New York, Cambridge University Press)
- Proffitt, C.R., & Quigley, M.F. 2001, *ApJ*, 548, 429
- Proust, D., Ochsenbein, F., & Pettersen, B.R., 1981, *A&AS*, 44, 179
- Ramspeck, M., Heber, U., & Edelmenn, H., 2001, *A&A*, 379, 235
- Robertson, J.G., Bedding, T.R., Aerts, C., et al., 1999, *MNRAS*, 302, 245
- Rodríguez Pascual, P.M., González-Riestra, R., Schartel, N., & Wemsteker, W. 1999, *A&AS*, 139, 183
- Ryans, R.S.I., Hambly, N.C., Dufton, P.L., & Keenan, F.P., 1996, *MNRAS*, 278, 132
- Sanner, J., Brunzendorf, J., Will, J.M., & Geffert, M., 2001, *A&A*, 369, 511
- Schartel, N., & Skillen, I. 1998, in *UV Astrophysics, Beyond the IUE Final Archive*, ed. W. Wamsteller & R. Gonzalez Riestra (ESTEC: Noordwijk), 735
- Shatsky, N., & Tokovinin, A., 2002, *A&A*, 382, 92
- Schrijvers, C., & Telting, J. H., 2002, *A&A*, 394, 603
- Shobbrook, R.R., & Robertson, J.W., 1968, *PASAu*, 1, 82
- Snijders, M.A.J., 1969, *A&A*, 1, 452
- Stankov, A., Handler, G., Hempel, M., & Mittermayer, P., 2003, *MNRAS*, 336, 189
- Thoul, A., Aerts, C., Dupret, M.A., et al., 2003, *A&A*, 406, 287
- Uytterhoeven, K., Aerts, C., De Cat, P., et al., 2001, *A&A*, 371, 1035
- Venn, K.A., Brooks, A.M., Lambert, D.L., Lemke, M., et al., 2002, *ApJ*, 565, 571

Table 1. The list of β Cephei stars. The names, HD numbers, the Hipparcos parallax, π , numbers of the IUE images used, sources of the ground-based data (last column) are given.

name	HD number	π [mas]	SWP camera	IUE numbers LWP camera	LWR camera	References
HN Aqr			23355, 37224, 37225, 37226, 37227, 37228, 37229, 37230, 37231	03661		6
γ Peg	886	9.79 ± 0.81	52770, 52772, 52775, 52777, 52783	29482, 29483, 29485, 29493, 29495		2, 3, 4, 5, 6
δ Cet	16582	5.04 ± 0.83	29807, 29808, 29809, 29810, 29811, 29812, 29813, 29814	06341, 09634, 09635, 09636, 09637		2, 3, 4, 5, 6
μ Eri	29248	5.56 ± 0.88	37958, 37959, 37960, 37961, 37962		04142	2, 3, 4, 5, 6
β CMa	44743	6.53 ± 0.66	42724, 42725, 42728, 42729, 42730, 42731, 42732, 42733, 42734, 42735, 42736	15384, 04531, 04532		1, 2, 3, 5, 6
ξ^1 CMa	46328	1.59 ± 0.70	19244		15280	2, 6
15 CMa	50707	2.02 ± 0.70	03575		02426, 02434, 01349	1, 2, 6
19 Mon	52918	2.92 ± 0.87	21913, 22113, 27665, 27757, 29239, 29348, 29385, 30393, 32115, 32399, 32926, 35104, 49291, 50412, 52939	07019		3, 4, 5, 6
27 CMa	56014	2.07 ± 0.59	03392, 02866		02979, 03402, 02543	2, 6
β Cru	111123	9.25 ± 0.61	05197, 05198, 05199, 05200 05201, 05202, 05203, 05204 05205		04502	2, 6
α Vir	116658	12.44 ± 0.86	50032, 18950, 33082, 33091	12841	13650, 15000	2, 3, 4, 5, 6
ϵ Cen	118716	8.68 ± 0.77	04347, 05707		03837	1, 2, 6
ν Cen	120307	6.87 ± 0.77	36481, 36482	24753		1, 2, 6
β Cen	122451	6.21 ± 0.56	17381		13628, 13629	1, 2, 6
τ^1 Lup	126341	3.15 ± 0.69	05206, 05207, 05208		04503	2, 6
α Lup	129056	5.95 ± 0.76	04564, 04565, 04566, 04567, 04568, 04569, 04573, 04574 16057, 16058	23572		1, 2, 6
BU Cir	129557	1.89 ± 0.69	07687		12353	6
V836 Cen	129929	1.48 ± 1.03	16770, 16775, 17457, 17458 16778		06697 13739	6 1, 6
β Lup	132058	6.23 ± 0.71	16770, 16775, 17457, 17458		13034	1, 6
δ Lup	136298	6.39 ± 0.86	16778			1, 6
ω^1 Sco	144470	7.70 ± 0.87	09237, 09239, 42228	20992		1, 6
σ Sco	147165	4.44 ± 0.81	45517	23843		2, 6
θ Oph	157056	5.79 ± 0.69	04421, 04422, 04423, 04424, 04425, 04426, 04427, 04428, 04429, 04430	24025		1, 2, 6
λ Sco	158926	4.64 ± 0.90	06270, 17385, 17398, 20627 12741, 12742, 12743	12737, 12738, 12739, 12740,		1, 2, 6
κ Sco	160578	7.03 ± 0.73	04323, 04348		03839	1, 6
V2052 Oph	163472	3.93 ± 0.97	50411, 50431, 50642, 50644, 50651, 50658, 50659, 52122, 55480, 55488, 55506, 55526, 55531, 55535, 55540, 55571, 55601, 55610, 55633, 55648, 55654, 55668, 55672, 55683, 55688, 55698, 55702, 55711, 55714, 55732, 55737, 55746, 55753, 55757, 55782, 55783, 50636, 50639, 18313, 14514, 14515		11089	1, 6
BW Vul	199140	1.84 ± 0.68	52642, 52643, 52644, 52648, 05590, 05591, 05597, 05598, 52847, 52848, 52849, 52850, 52851, 52852, 52853, 52854, 52855, 52856, 52862, 52863, 52864, 52865, 52866, 52867, 52868, 52869, 52870, 52871, 52877, 52878, 52879, 52880, 52881, 52882, 52883, 52884, 52885		04843, 04844, 04845, 04846	6
SY Equ	203664	2.23 ± 1.08	07354, 07355, 37035, 37036, 51083, 51084, 51085, 51086, 10069	16368, 16369, 28408, 28409, 28410	06346, 06347, 08764	6
β Cep	205021	5.48 ± 0.47	46186, 46255, 52514, 42785, 42800, 42825, 46153, 52415, 52460, 52488, 52547, 52573, 52594, 52620, 52653, 53911	19491		2, 3, 4, 5, 6
12 Lac	214993	2.34 ± 0.62	42631	21420, 31313		6
16 Lac	216916	2.71 ± 0.69	05354, 05355, 05357, 05358, 05359, 05360, 05361		04599	6

References: 1 – Alekseeva et al. (1996), 2 – Breger (1976), 3 – Glushneva et al. (1998), 4 – Glushneva et al. (1992), 5 – Kharitonov et al. (1988), 6 – Mermilliod et al. (1997).

Table 2. The list of β Cephei stars belonging to open clusters. ID numbers, names and numbers of the used IUE images are given.

ID Number	Name	IUE numbers	
		SWP camera	LWP/LWR camera
N3293-10	V401 Car	20306, 23759	16221
N3293-11		21527	16996
N3293-14	V405 Car	21513, 23568	16995
N3293-27	V380 Car	20307, 23758	16228
N3293-65	V412 Car	20324	16248
N3293-23	V404 Car	21529, 23570	16998
N4755-III-1	CT Cru	33701	13352
N4755-I-13		33702	13355
N4755-I	CV Cru	33703	13356
N4755-G	BS Cru	33709	13365
N4755-F	BW Cru	36249	15505
N6231-110	V947 Sco	02762	02464
N6231-150	V920 Sco	24120	04503
N6231-238	V964 Sco	16593	12829
N6231-261	V946 Sco	24119	04502
N6231-282	V1032 Sco	16606	12846

Table 3. The best-fit parameters for the β Cephei stars obtained from the IUE/NEWSIPS low-resolution data.

HD	Name	$\log T_{\text{eff}}$	$\log g$	[m/H]	θ [mas]	$E(B - V)$ [mag]
–	HN Aqr	4.332 ± 0.018	4.10	0.21 ± 0.09	0.009 ± 0.000	0.068 ± 0.010
886	γ Peg	4.342 ± 0.011	3.82	-0.04 ± 0.08	0.427 ± 0.011	0.010 ± 0.005
16582	δ Cet	4.339 ± 0.014	3.73	-0.24 ± 0.09	0.246 ± 0.009	0.014 ± 0.006
29248	μ Eri	4.373 ± 0.016	3.78	0.05 ± 0.09	0.257 ± 0.011	0.059 ± 0.010
44743	β CMa	4.392 ± 0.014	3.74	0.04 ± 0.10	0.581 ± 0.023	0.023 ± 0.009
46328	ξ^1 Cma	4.383 ± 0.021	3.89	-0.33 ± 0.19	0.197 ± 0.011	-0.003 ± 0.010
50707	15 CMa	4.391 ± 0.018	3.81	0.05 ± 0.10	0.160 ± 0.008	0.041 ± 0.010
52918	19 Mon	4.380 ± 0.015	3.96	0.15 ± 0.10	0.156 ± 0.006	0.046 ± 0.009
56014	27 CMa	4.397 ± 0.022	4.18	-0.47 ± 0.18	0.173 ± 0.010	0.087 ± 0.012
111123	β Cru	4.413 ± 0.020	3.75	-0.14 ± 0.13	0.752 ± 0.040	-0.002 ± 0.011
116658	α Vir	4.392 ± 0.012	3.70	-0.12 ± 0.08	0.921 ± 0.031	0.020 ± 0.005
118716	ϵ Cen	4.387 ± 0.023	3.72	-0.14 ± 0.10	0.504 ± 0.029	0.019 ± 0.012
120307	ν Cen	4.360 ± 0.017	3.85	-0.26 ± 0.10	0.322 ± 0.013	0.013 ± 0.007
122451	β Cen	4.408 ± 0.020	3.89	-0.03 ± 0.15	1.074 ± 0.059	0.028 ± 0.009
126341	τ^1 Lup	4.356 ± 0.023	3.74	-0.39 ± 0.16	0.217 ± 0.010	0.101 ± 0.026
129056	α Lup	4.357 ± 0.015	3.57	0.04 ± 0.10	0.558 ± 0.030	0.045 ± 0.007
129557	BU Cir	4.386 ± 0.028	3.92	-0.27 ± 0.11	0.126 ± 0.028	0.238 ± 0.090
129929	V836 Cen	4.380 ± 0.022	3.92	-0.05 ± 0.10	0.040 ± 0.003	0.086 ± 0.010
132058	β Lup	4.361 ± 0.008	3.65	-0.35 ± 0.11	0.457 ± 0.008	0.039 ± 0.006
136298	δ Lup	4.354 ± 0.010	3.69	-0.25 ± 0.11	0.352 ± 0.007	0.023 ± 0.006
144470	ω^1 Sco	4.445 ± 0.010	4.11	-0.45 ± 0.15	0.291 ± 0.006	0.250 ± 0.008
147165	δ Sco	4.410 ± 0.025	3.86	-0.20 ± 0.20	0.597 ± 0.025	0.360 ± 0.032
157056	θ Oph	4.347 ± 0.016	3.77	-0.15 ± 0.12	0.350 ± 0.014	0.017 ± 0.008
158926	λ Sco	4.381 ± 0.011	3.69	-0.21 ± 0.08	0.731 ± 0.022	0.048 ± 0.006
160578	κ Sco	4.365 ± 0.010	3.62	-0.19 ± 0.10	0.501 ± 0.011	0.025 ± 0.007
163472	V2052 Oph	4.368 ± 0.012	3.89	-0.25 ± 0.16	0.177 ± 0.003	0.393 ± 0.011
199140	BW Vul	4.362 ± 0.017	3.71	0.07 ± 0.12	0.093 ± 0.020	0.145 ± 0.079
203664	SY Equ	4.379 ± 0.036	3.90	-0.01 ± 0.21	0.031 ± 0.004	0.060 ± 0.014
205021	β Cep	4.383 ± 0.015	3.69	-0.07 ± 0.10	0.320 ± 0.013	0.002 ± 0.007
214993	12 Lac	4.373 ± 0.020	3.65	-0.20 ± 0.10	0.175 ± 0.041	0.181 ± 0.089
216916	16 Lac	4.359 ± 0.033	3.90	-0.13 ± 0.13	0.137 ± 0.013	0.118 ± 0.018
N3293-10	V401 Car	4.370 ± 0.050	3.91	-0.14 ± 0.12	0.027 ± 0.003	0.276 ± 0.027
N3293-11	–	4.347 ± 0.022	3.84	-0.10 ± 0.12	0.023 ± 0.002	0.211 ± 0.012
N3293-14	V405 Car	4.352 ± 0.023	4.18	0.15 ± 0.11	0.027 ± 0.002	0.171 ± 0.010
N3293-23	V404 Car	4.340 ± 0.026	3.94	0.27 ± 0.06	0.075 ± 0.005	0.324 ± 0.016
N3293-27	V380 Car	4.393 ± 0.043	3.91	0.06 ± 0.10	0.039 ± 0.005	0.318 ± 0.019
N3293-65	V412 Car	4.354 ± 0.034	3.97	0.03 ± 0.11	0.022 ± 0.002	0.228 ± 0.016
N4755-F	BW Cru	4.397 ± 0.010	3.67	-0.31 ± 0.15	0.040 ± 0.002	0.409 ± 0.009
N4755-G	BS Cru	4.439 ± 0.020	3.87	-0.56 ± 0.20	0.027 ± 0.002	0.432 ± 0.015
N4755-I	CV Cru	4.393 ± 0.016	3.68	-0.29 ± 0.10	0.033 ± 0.002	0.569 ± 0.016
N4755-I-13	–	4.423 ± 0.013	4.03	-0.49 ± 0.12	0.024 ± 0.001	0.463 ± 0.012
N4755-III-1	CT Cru	4.411 ± 0.013	3.74	-0.50 ± 0.18	0.031 ± 0.002	0.437 ± 0.015
N6231-110	V947 Sco	4.400 ± 0.059	4.05	-0.03 ± 0.23	0.044 ± 0.007	0.495 ± 0.019
N6231-150	V920 Sco	4.409 ± 0.026	3.90	-0.21 ± 0.19	0.038 ± 0.005	0.459 ± 0.016
N6231-238	V964 Sco	4.438 ± 0.040	4.17	0.05 ± 0.15	0.037 ± 0.005	0.396 ± 0.021
N6231-261	V946 Sco	4.391 ± 0.025	3.95	0.01 ± 0.13	0.028 ± 0.004	0.435 ± 0.015
N6231-282	V1032 Sco	4.419 ± 0.028	3.76	-0.42 ± 0.16	0.038 ± 0.003	0.372 ± 0.012

Table 4. The best-fit parameters specifying the shape of the UV extinction curve and parameters of the standard extinction curve (Fitzpatrick (1999)).

HD	γ [μm^{-1}]	x_0 [μm^{-1}]	c_2	c_3	c_4
	0.99	4.596	0.698	3.23	0.41
126341	0.72 ± 0.13	4.542 ± 0.031	0.893 ± 0.377	1.86 ± 0.72	0.03 ± 0.25
129557	0.82 ± 0.05	4.580 ± 0.010	0.579 ± 0.315	2.66 ± 1.30	0.11 ± 0.18
144470	0.87 ± 0.06	4.582 ± 0.012	0.866 ± 0.108	2.90 ± 0.33	0.15 ± 0.10
147165	0.94 ± 0.04	4.572 ± 0.007	0.326 ± 0.067	3.20 ± 0.25	0.19 ± 0.06
163472	0.65 ± 0.03	4.539 ± 0.007	0.562 ± 0.073	2.22 ± 0.17	0.18 ± 0.11
199140	0.77 ± 0.08	4.611 ± 0.021	0.875 ± 0.570	1.97 ± 1.29	0.20 ± 0.11
214993	0.86 ± 0.08	4.606 ± 0.024	0.776 ± 0.327	1.75 ± 0.79	0.10 ± 0.21

Table 5. The mean correlations, ρ_{mean} , their standard deviations, σ_ρ , median values, ρ_m , and ranges of correlation coefficients between the determined parameters.

$\rho(p_i, p_j)$	ρ_{mean}	ρ_m	σ_ρ	Range of ρ	
$\rho(\theta - T_{\text{eff}})$	0.657	0.784	0.296	0.011	0.972
$\rho(\theta - E(B - V))$	0.443	0.435	0.271	0.001	0.963
$\rho(\theta - [\text{m}/\text{H}])$	0.226	0.185	0.170	0.002	0.656
$\rho(\theta - S_1)$	0.525	0.605	0.274	0.001	0.996
$\rho(\theta - S_2)$	0.579	0.696	0.292	0.004	0.996
$\rho(T_{\text{eff}} - \theta)$	0.657	0.784	0.296	0.011	0.972
$\rho(T_{\text{eff}} - E(B - V))$	0.726	0.768	0.184	0.020	0.959
$\rho(T_{\text{eff}} - [\text{m}/\text{H}])$	0.261	0.217	0.189	0.001	0.749
$\rho(T_{\text{eff}} - S_1)$	0.577	0.668	0.248	0.029	0.945
$\rho(T_{\text{eff}} - S_2)$	0.500	0.534	0.223	0.039	0.880
$\rho(E(B - V) - \theta)$	0.443	0.435	0.271	0.001	0.963
$\rho(E(B - V) - T_{\text{eff}})$	0.726	0.768	0.184	0.020	0.959
$\rho(E(B - V) - [\text{m}/\text{H}])$	0.186	0.157	0.141	0.002	0.794
$\rho(E(B - V) - S_1)$	0.333	0.305	0.207	0.007	0.862
$\rho(E(B - V) - S_2)$	0.271	0.204	0.212	0.005	0.859
$\rho([\text{m}/\text{H}] - \theta)$	0.226	0.185	0.170	0.002	0.656
$\rho([\text{m}/\text{H}] - T_{\text{eff}})$	0.261	0.217	0.189	0.001	0.749
$\rho([\text{m}/\text{H}] - E(B - V))$	0.186	0.157	0.141	0.002	0.794
$\rho([\text{m}/\text{H}] - S_1)$	0.267	0.195	0.225	0.003	0.881
$\rho([\text{m}/\text{H}] - S_2)$	0.166	0.128	0.129	0.001	0.549
$\rho(S_1 - \theta)$	0.525	0.605	0.274	0.001	0.996
$\rho(S_1 - T_{\text{eff}})$	0.577	0.668	0.248	0.029	0.945
$\rho(S_1 - E(B - V))$	0.333	0.305	0.207	0.007	0.862
$\rho(S_1 - [\text{m}/\text{H}])$	0.267	0.195	0.225	0.003	0.881
$\rho(S_1 - S_2)$	0.860	0.886	0.116	0.500	1.000
$\rho(S_2 - \theta)$	0.579	0.696	0.292	0.004	0.996
$\rho(S_2 - T_{\text{eff}})$	0.500	0.534	0.223	0.039	0.880
$\rho(S_2 - E(B - V))$	0.271	0.204	0.212	0.005	0.859
$\rho(S_2 - [\text{m}/\text{H}])$	0.166	0.128	0.129	0.001	0.549
$\rho(S_2 - S_1)$	0.860	0.886	0.116	0.500	1.000